Cement & Concrete Composites 31 (2009) 84–91

Contents lists available at ScienceDirect

Cement & Concrete Composites

journal homepage: www.elsevier.com/locate/cemconcomp

Shape assessment of particles in concrete technology: 2D image analysis and 3D stereological extrapolation

P. Stroeven, J. Hu, Z. Guo *

Faculty of Civil Engineering and Geosciences, Delft University of Technology, Stevinweg 1, 2628 CN Delft, The Netherlands

ARTICLE INFO

Article history:
Received 22 June 2006
Received in revised form 10 September 2008
Accepted 11 September 2008
Available online 20 September 2008

Keywords:
Concrete aggregate
Shape assessment
Quantitative image analysis
Stereology

ABSTRACT

A survey is given of stereology-based two-dimensional (2D) and three-dimensional (3D) approaches to shape assessment of embedded or non-embedded particles. Firstly, the development is outlined of global parameters characterizing geometric structure of cementitious materials. Secondly, these parameters are combined to yield effective shape estimators to be applied to section images of embedded particles or to projection images of non-embedded particles. This application can be just 2D, denoted as quantitative image analysis, giving information on what is displayed of the particle(s) in the section or projection image plane only. However, the researcher should strive for geometrical–statistical (stereological) extrapolation of the 2D observations to the real world's third dimension. This is demonstrated superior over the 2D approach, however, requires a careful sampling strategy for providing representative information on structure.

1. Introduction

Quantitative characterization of geometric features of material structure is nowadays more common because of the recognition that material performance depends on material structure. The most obvious parameter in such approaches is *material density*; the investigator is interested in how much of a certain component (here: aggregate) is incorporated in the relevant material system. Stereological methods render possible deriving three-dimensional unbiased estimates of material density (or of more complicated geometric features) from observations on *representative* two-dimensional section or projection images.

The next question raised could be: "how to optimize density"? This question is on engineering level commonly quite crudely approached by investigating the effect of the aggregate sieve curve on maximum density of the aggregate. In doing so, it is assumed that sieve opening can be associated with *particle size*. Optimum density of particles in blended Portland cement binders can result in significant physical (in addition to chemical) contributions to mechanical performance of (super) high performance concrete systems [1–3]. This is achieved by carefully designing such binder mixtures on the basis of size ranges of particle components [4]. Hence, size is an important geometric measure of particles. This is not a trivial measurement. Size can be unambiguously fixed for spheres, of course. But for arbitrarily shaped particles, determination of size would require agreement on the applied definition.

An argument to introduce a paper on *shape* by starting with size is the intimate relationship that exists between these geometric features. Supposedly, the size distribution of an aggregate is studied in section or projection images. It must be quite obvious, however, that the two-dimensional size distribution function that can be obtained in such section or projection planes can only be transferred to the three-dimensional level *when particles are of a similar shape*. So, size and shape assessment are related topics, indeed. And both affect the density in the jammed state of aggregate grains.

The underlying crude size assessment method (sieving) makes it impossible, unfortunately, experimentally assessing shape effects on compaction density [5]. Yet, when crushed rock would be employed as aggregate, the rough surface texture and irregular shape will hamper achieving the same packing density as achieved with river aggregate [6]. As a consequence, porosity characteristics that govern durability performance are influenced [7]. So, particle shape and surface texture should be considered important geometric features in concrete technology. Of course, this is a sole example of the technological relevance of these parameters. Methods for assessing *surface roughness* of aggregate grains, mostly considered part of shape analysis, are readily available. Local values of surface amplitude are determined along traces at the surface of the grain. The root mean square value of surface amplitude data with respect to a smooth reference surface is directly linked up with the surface roughness. Stereological methods are based on scanning representative profiles in section or projection images with a sweeping test line system [8,9]. Next, the profile roughness, R_L, is related to the surface roughness, R_S [9–11].

* Corresponding author. Tel.: +31 15 2785835; fax: +31 15 2788162.
E-mail address: z.guo@tudelft.nl (Z. Guo).

0958-9465/$ - see front matter © 2008 Elsevier Ltd. All rights reserved.
doi:10.1016/j.cemconcomp.2008.09.006

Hence, this leaves the complicated problem of assessing the shape of particles, in the first place of aggregate grains, but also of binder particles, when relevant in the technological approach. As to assessment of geometric properties, "this is the most indeterminate subject of all" [8, p. 195]. Or, in the words of Kendall, et al: "Everyone knows what is meant by 'shape'. However, it is not a trivial matter to define shape in a manner that is susceptible to mathematical and statistical analysis" [12, Preface]. As argued earlier, size and shape both vary simultaneously in practice. Only when both geometric parameters are unambiguously defined, we can explore technological problems more thoroughly, whereby size and shape both play a role.

This problem has been studied more extensively outside the field of concrete technology, so one could profit from experiences and resulting progress achieved in such fields. As with particle size, the problem has two faces. In the first case, loose particles are available for further study. Generally, projection images are prepared from the particles. Dimensions can range from mesoscopic to microscopic ones. Shape can be derived from simple measurements, when certain conditions are fulfilled. The second problem arises when such particles are embedded in an opaque cementitious matrix. So, two-dimensional section (or thin sections projection) images are available for the assessment of shape characteristics. The 2D section and projection images can be employed in a direct approach, whereby so called *descriptors* of particles are obtained. Alternatively, the obtained data are 'extrapolated' by stereological methods into 3D space; hence, stereological methods allow correlating descriptors derived from 2D images to descriptors pertaining to 3D space. The 2D approach offers the more intuitive and, hence, the more frequently used route.

Stereological methods will be of innovative nature for many researchers. Nevertheless, the stereological approach to shape assessment will be demonstrated later being more versatile and more sensitive so can be considered superior over the 2D approaches. Hence, using stereological methods for shape assessment would be a step forward over the more pragmatic methods employed nowadays [13]. Not the last step though; Fast Fourier Transform offers additional and even more promising possibilities [13]. We will come back to this advanced approach in a next publication.

Shape assessment starts by describing particles as revealed in 2D images, either obtained from sections or from projections. We will present lists of such descriptors that could play a role in characterizing shape. Next, a list of descriptors pertaining to 3D space is presented that could be employed in a 3D shape assessment approach. Both types of descriptors can be correlated by stereological relationships that will be presented and briefly discussed next. Finally, shape analysis concepts of 2D and 3D nature will be presented in which several of the aforementioned descriptors are combined. Applications to section images of embedded particles are more common in the literature than to projection images. So, this paper will present as *illustrative material* an example of shape assessment on the basis of projection images of loose particles of river aggregate and crushed rock, respectively.

2. Descriptors of particles in 2D and 3D

Embedded particles show up in random 2D sections as dispersed areas of various sizes separated from the surrounding matrix by their perimeters. The same holds for loose particles in the 2D projection images, matrix being void, of course (Fig. 1). The observed perimeters are resorting under the more general category of *lineal features or traces in the two-dimensional plane*. Also cracks lead to lineal traces in the section plane. So, traces may form closed, isolated areas, as in the present case of aggregate particles, but in general can also form network elements. Researchers may be interested in geometric characteristics of these lineal features, such as total trace length, or trace length of network elements, and planar orientation distribution. Also, planar spacing could be a feature of interest. Descriptors will deal specifically with the closed perimeter loop of a *particle*, whereby enclosed area (A), loop length (L_p), linear extension in a certain direction (H), length of a straight randomly on the loop superimposed line (L_2), local curvature (k_L), or degree of orientation (ω_2) can be measured. Descriptors are averaged over the various particles in section or projection images. However, *without bestowing extra efforts* on data extraction, also three-dimensional structure information can be obtained. Instead, extra attention should be paid to the sampling strategy that should provide the representative images subjected to data extraction [14–17]. We will come back to this crucial issue in the framework of presenting the stereological methods.

2.1. Descriptors that can be obtained from 2D section images of embedded particles

- $\bar{A}$ (mm^2) – average area of particle sections (Fig. 2a);
- $\bar{L}_p$ (mm) – average perimeter length of particle sections (Fig. 2a);
- $\bar{H}_2$ (mm) – average tangent height of particle sections (Fig. 2b);

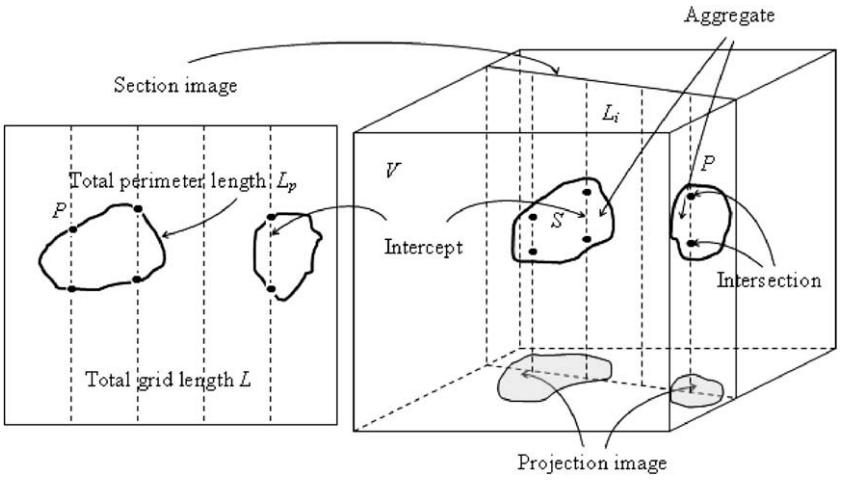

Fig. 1. Assessment of length of lineal features (perimeters of particles) in plane (left) and of specific surface area (of aggregate grains) in space (right), both by line scanning and intersection (or intercept) counting.

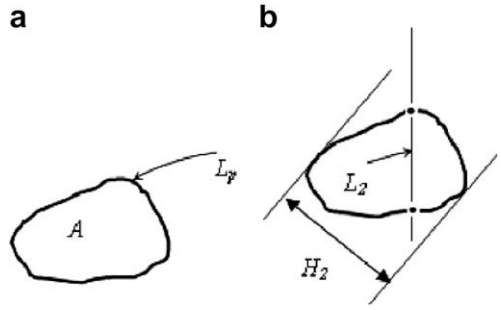

Fig. 2. Descriptors obtained from section image.

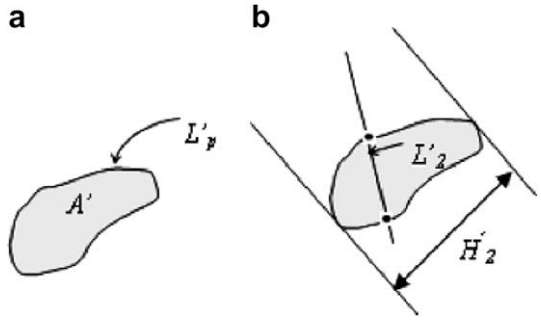

Fig. 3. Descriptors obtained from projection image: particle in cube is projected onto bottom surface. Perimeter length can be obtained through Eq. (2). Random lines form intercepts, L_3, and yield intersection point densities, P_L. The projected area of the particle can be determined through Eq. (1) by point sampling.

- $\bar{L}_2$ (mm) – average intercept length of particle sections (Fig. 2b);
- $\bar{k}_L$ – mean curvature of particle perimeters;
- $\bar{\omega}_2$ – average degree of orientation of particle perimeters.

2.2. Descriptors that can be obtained from 2D projection images of loose particles

- $\bar{A}'$ (mm^2) – average area of particle projections (Fig. 3a);
- $\bar{L}'_p$ (mm) – average perimeter length of particle projections (Fig. 3a);
- $\bar{H}'_2$ (mm) – average tangent height of particle projections (Fig. 3b);
- $\bar{L}'_2$ (mm) – average intercept length of particle projections (Fig. 3b);
- $\bar{k}'_L$ – mean curvature of particle perimeters;
- $\bar{\omega}'_2$ – average degree of orientation of particle perimeters.

Note that projected features are indicated by a prime (′).

2.3. Descriptors of spatial nature that can be obtained from section and/or projection images

- $\bar{V}$ (mm^3) – average volume of particle(s);
- $\bar{S}$ (mm^2) – average surface area of particle(s);
- $\bar{H}_3$ (mm) – average tangent height of particle(s);
- $\bar{L}_3$ (mm) – average intercept length of particle(s);
- $\bar{k}_S$ – average mean curvature of particle surface(s);
- $\bar{\omega}_3$ – average degree of orientation of particle(s).

3. Stereological relationships between descriptors pertaining to 2D and 3D, respectively

3.1. Volume fraction of particles V_V

Behavior and performance are always governed by '*how much*' of the component at issue (particles) is incorporated in the cementitious material. The experimental methodology to find out is based on superposition of line or point grids on field images of (part of) sections. The fraction of such lines, L_L, or points, P_P, covering the component of interest (here, particle sections) is an unbiased estimator of volume fraction [18]. So, for an embedded aggregate we have

$$\bar{A}_A = \bar{P}_P = \bar{L}_L = V_V \tag{1}$$

in which the bar on top of the symbols denote proper averaging procedures. This is accomplished on a representative set of images provided by the selected sampling strategy. For loose particles, more direct methods are available for volume fraction determination.

3.2. Specific surface area of particles S_V

Superposition of a line grid on a field image additionally allows determination of the number of intersections with the traces (perimeter) due to particles. Trace length per unit of the sampled area, L_A, is directly related to the average number of intersections per unit of grid line length, $\bar{P}_L$, by

$$\bar{P}_L = \frac{2}{\pi} L_A \tag{2}$$

This formula goes back to Cauchy [18] and was used for the present purpose by Steinhaus [19]. Its three-dimensional equivalence relates $\bar{P}_L$, or the average number of intercepts per unit of test line length, $\bar{N}_L$, to S_V

$$\bar{P}_L = 2\bar{N}_L = \frac{1}{2} S_V \tag{3}$$

The planar and spatial averaging procedures on which the unbiased estimates rely (see Appendix A) lead to the constant factors in Eqs. (2) and (3). Efficiency of the approach is high [20,21].

When loose particles are projected in parallel light (Fig. 4), the mean projected area of particles, $\bar{A}'$, can be assessed. The surface of a single (convex) aggregate particle, S, is related to $\bar{A}'$ by the Cauchy expression

$$4\bar{A}' = S \tag{4}$$

3.3. Rose-of-intersections $P(\theta)$, or total projections $L'(\theta)$

The sweeping test line approach to field images leads to a so-called rose-of-intersections, or rose-of-intersection densities, $P_L(\theta)$. Since according to the total projection rule,

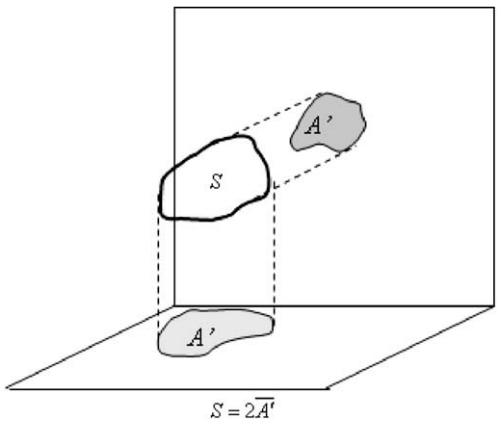

Fig. 4. Assessment of surface area by areal analysis, i.e., by subjecting the projection image to methods of Eq. (1). In the case of a closed convex surface of a particle, total projection of its surface will be twice the measured area A' So, the expression $4\bar{A}' = S$ is commonly used. For non-convex particles, one has to additionally account for *total projections* when using this formula.

$$P_L(\theta) = L'_A\left(\theta + \frac{\pi}{2}\right) \tag{5}$$

roses-of-intersection densities $P_L(\theta)$ and of total projected length per unit of area L'_A are similar, however rotated 90° with respect to each other [23]. The rose would approximate a circle when confronted with 'randomly' dispersed surfaces in space (here: aggregate of spherical particles). The rose will get elongated for surfaces with preferred orientation. Of course, smooth shaped roses are only obtained for representative samples. For individual fields, the roses have an irregular shape.

The average radius of the rose-of-intersection density is, in agreement with Eq. (2), proportional to the total perimeter length of particle sections. Maximum and minimum values are used to define the *average degree of orientation* of the traces in the plane, $\bar{\omega}_2$. The spatial value of the degree of orientation, $\bar{\omega}_3$, can be based on the same two measurements, however. For specific information the reader is referred to the relevant literature [18,21]. The degrees of orientation depend obviously on the non-spherical shape characteristics of the aggregate particles.

The same approach can also be used to define the shape of a single object or of a series of objects (e.g., loose particles). The two-dimensional shadow image is therefore subjected to a directed secants analysis. The ratio of maximum and minimum rose dimensions is as in the section case related to particle shape.

3.4. Tangent height H_2 in 2D

The tangent height of a particle in a direction θ is the projected length of the particle's perimeter in a perpendicular direction. The following relationship exists

$$H_2(\theta)N_A = N_L(\theta + \pi/2) \tag{6}$$

in which N_A is the number of particle sections per unit of area, and N_L is the number of such sections hit by a system of parallel lines. H_2 is the shadow height perpendicular to this line system. This operation can be repeated for various values of θ to yield a rose of tangent heights, which is related to the shape of the aggregate. Averaging over θ gives

$$\bar{H}_2 = \frac{\bar{N}_L}{N_A} \tag{7}$$

This expression correlates the number of particle sections hit by random secants per unit of test line length, the number of particle sections per unit of area, and the average size of particle sections. For embedded or loose particles, this approach is used to define *shape*. To that end, the ratio of maximum and minimum values of $H_2(\theta)$ is employed. We will come back to this later.

3.5. Tangent height H_3 in 3D

This parameter is used in an analogous way as its two-dimensional equivalent. For single particles (or a group of non-embedded particles with similar shape, but eventually with different sizes), a random set of shadow pictures is produced and maximum and minimum values of tangent height assessed. The ratio can be used as *shape* parameter as we will see later. Average tangent height is related to size of particles by a relationship analogous to Eq. (7)

$$\bar{H}_3 = \frac{N_A}{N_V} \tag{8}$$

in which $\bar{H}_3 = \bar{d}$, the average particle diameter, when also N_A is averaged over a set of randomly oriented sections. Problem is that N_V cannot easily be determined unless confronted with a translucent matrix.

3.6. Mean intercept lengths $\bar{L}_2$ in 2D and $\bar{L}_3$ in 3D

These parameters are primarily used to define *size* of non-spherical particles. The indices $\bar{L}_2$ and $\bar{L}_3$ refer to application in two-dimensions (plane) and in three-dimensions (space), respectively. The mean intercept length is the total length of random intercepts divided by the number of intercepts. We have

$$\bar{L}_2 = \bar{L}_3 = \frac{L_L}{N_L} = \frac{P_P}{N_L} \tag{9}$$

in which L_L is the total intercept length per unit of test line length, and P_P the point ratio of particles hitting the section area to the total number applied, and N_L is the number of intercepts per unit of test line length. This concept is directly related to ASTM grain size number [25].

3.7. Equivalent area circle

The average section area of dispersed particles is denoted by $\bar{A}(= A_A/N_A)$. The equivalent circle has the same area. So,

$$\bar{A} = \frac{1}{4}\pi d_{eq}^2 \tag{10}$$

This defines two equivalent length measures, diameter d_{eq} and perimeter length of the equivalent circle Lp_{eq}, respectively. They are both applied in shape analysis, as we will see later.

3.8. Average mean curvature

The local mean curvature, k_S, is the local average of principal curvatures (in orthogonal planes) at the surface, i.e. $k_S = \frac{1}{2}(k_1 + k_2)$. The *integral mean curvature* is the value of k_S integrated over the total surface area of a particle, S, or of a group of embedded particles, $\bar{S}$. It is found that the average mean curvature for surfaces in space (3D approach) is given by [22]

$$\bar{k}_S = \frac{\pi N_A}{2N_L} \tag{11}$$

The same operation can be accomplished in the 2D case for traces (perimeter of particles) in a plane with the solution (with zero value for either k_1 or k_2) [22]

$$\bar{k}_L = \frac{2N_A}{N_L} \tag{12}$$

3.9. Sampling strategy

Averaging operations in 2D (section or projection images) should be accomplished by randomly changing orientation. When the 3D assessment of characteristics of structure is targeted (based on similar 2D section or projection images), the randomization operation should be extended in 3D space. This is very unpractical for embedded aggregate, but can easily be accomplished for loose particles, of course. Note that images of which orientation is defined by $\{\alpha, \beta\}$ require randomization of β and $\sin\alpha$ [18]! See also Appendix A.

Fortunately, in many cases it is possible defining an axis of symmetry as to the dispersed surfaces of the aggregate grains. Under such conditions, the image analysis operations can be restricted to only *vertical sections*, i.e. sections parallel to the axis of symmetry. This is significantly simplifying the procedure, of course. Still, superposition of lineal grids should be avoided. Instead, a grid system of staggered cycloids should be used for intersection counting. This accounts for the sine-weighed orientation distribution involved in the spatial averaging operation, as stipulated earlier [18]. Alternatively, further assumptions can be made as to the

spatial dispersion of surfaces, as conventionally applied by Stroeven [23], following a suggestion by Saltikov [24]. This further simplifies the quantitative image analysis procedure to two orthogonal measurements with directed secants in the vertical section.

4. Shape analysis

As argued earlier, shape is one of the most difficult features to define. And, without definition, quantification is impossible. Different procedures are therefore followed for arriving at more particular solutions. The ASTM grain size chart is an example of linking up three-dimensional grain shape discretely with for the field of application relevant series of typical section shapes [25]. For a single *non-embedded particle*, shape can be defined, but averaging for an aggregate would require doing so for volumes and surfaces of particles. Since these operations are scale dependent, this will generally not lead to manageable solutions. Most of the research on this topic has been focusing on characterizing by stereological means two-dimensional sections through embedded particles, a situation that can be considered pertinent for cementitious materials. A special case is serial sectioning with the objective of three-dimensional reconstruction; an extremely labor-intensive approach for opaque materials like concrete. Anatomists and biologists have extensively developed this technique for *translucent* samples. Less frequently accomplished is shape characterization of non-embedded particles by projected images. An alternative option is the generation of mathematically defined two-dimensional sections or three-dimensional surfaces as a reference for estimating shape of actual geometric elements of structure.

4.1. Shape analysis on 2D section images

The following are some simple shape parameters, whose usefulness depends on the problem at issue. They can be used for single particles or an aggregate of *similarly shaped particles*, whereby the particle size distribution function will be accounted for as discussed later.

- L/W – length to width ratio (L and W in oblique directions);
- $\bar{L}_P/\bar{L}_2$ – average perimeter length divided by the average intercept length;
- $\bar{L}_P^2/\bar{A}$ – average perimeter length squared divided by the average cross sectional area;
- $\overline{Ak}_L^2$ – average cross sectional area times the average line curvature squared;
- $\bar{L}_P/L_{Peq}$ – ratio of average perimeter length and perimeter length of the equivalent circle;
- $\bar{L}_2/\bar{L}_{2eq}$ – ratio of average intercept length and average intercept length of the equivalent circle;
- Note that $\bar{L}_{2eq} = L_L/N_L = 4V_V/S_V$.

4.2. Shape analysis on 2D projection images

Shape estimates can also be based on projected images or silhouettes of *non-embedded* particles. They can be used for single particles or an aggregate of *similarly shaped* particles, whereby the particle size distribution function will be accounted for as discussed later.

- L'/W' – Elongation ratio (L' and W' in oblique directions);
- $(L'_p)^2/(4\pi * A')$ – Circularity;
- $A'/(\text{Area of bounding rectangle})$ – Rectangularity;
- $H'_{2\max}/H'_{2\min}$ – Aspect ratio;
- $A'/(H'_{2\max} * H'_{2\min})$ – Fullness.

where $H'_{2\max}$ and $H'_{2\min}$ are maximum and minimum values of tangent height or Feret diameter, respectively (Fig. 5).

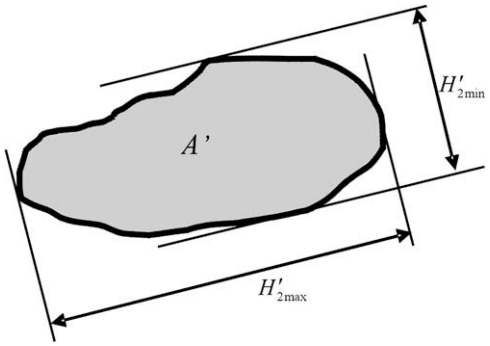

Fig. 5. Maximum and minimum values of tangent height in the projection plane.

The above-mentioned parameters are self-explanatory. The circularity and rectangularity describe the extent of approximation of the particle shadow profile to circle and to rectangle, respectively. However, these shape descriptors cannot regenerate the original shape of the projection profiles since these parameters contain no information as to the boundary variations of the profiles. The study of Yamamoto et al. [26] revealed that conventional parameters such as circularity are far from efficient descriptors of irregular geometrical shapes. Based on the assumption that aggregate particles from the same source should have more or less similar shape characteristics, a global parameter reflecting the correlation between mean thickness and measurable dimensions (e.g., breadth) of the particles has been introduced in a quasi-stereological (hence, 3D) approach to projection images. Kwan et al. [27] proposed a global flakiness ratio (λ) defined as the weight-averaged ratio of thickness to breadth of the aggregate particles. The total volume (V) and the mass (M) of the particles can be expressed as

$$V = \sum_{i=1}^{n}(\text{thickness} \times \text{area}) = \lambda \times \sum_{i=1}^{n}(\text{breadth} \times \text{area}) \tag{13}$$

$$\lambda = \frac{M}{\rho \times \sum_{i=1}^{n}(\text{breadth} \times \text{area})} \tag{14}$$

where ρ is the specific gravity density of the aggregate grains, and n is the number of aggregate grains in the sample. The parameter λ may serve as a flakiness indicator and its value can be calculated via Eq. (14) since total mass of the sample (M), breadth and projection area of each particle can be determined by image analysis. This allows defining the following quasi-3D parameters based on quantitative (projection) image analysis

$$\text{Flakiness ratio } (\lambda) = \text{Thickness/breadth}$$

$$\text{Sphericity ratio} = 3\sqrt{\lambda(\text{breadth/length})^2}$$

$$\text{Shape factor} = \lambda\sqrt{\text{breadth/length}}$$

4.3. Stereological approach to 3D shape assessment

Shape factors or shape indices can be formed (and have been used) from combinations of the earlier listed stereological descriptors. The proper combinations should be attuned to the problem at issue. For aggregate particles, the approximate size distribution function, $f_i(d)$, can be derived from the sieve curve. For examples of the Fuller and constant volume fraction mixes, see Stroeven [28]. Moments of the size distribution function are obtained from

$$M_n(d) = \frac{\sum_i^m d^n f_i(d)}{\sum_i m f_i(d)} \tag{15}$$

in which the histogram of particle sizes encompasses m classes. The three-dimensional stereological descriptors are related to the appropriate moments of the common particle size distribution function. This can be formulated in the following way:

$$\bar{V} = s_3 M_3$$
$$\bar{S} = s_2 M_2$$
$$\bar{H}_3 = s_1 M_1 \quad \text{or} \quad \bar{L}_3 = s_1^* M_1(d)$$
$$\bar{k}_S = s_{-1} M_{-1}$$

in which s_3, s_2, s_1, s_1^* and s_{-1} are dimensionless form factors. Underwood presented combinations of such form factors as shape indices [29]. The most relevant for the present case is (see also Appendix B)

$$\frac{s_2^2}{s_1 s_3} = \frac{4P_L^2}{N_A P_P} \frac{M_1(d) M_3(d)}{M_2^2(d)} \tag{16}$$

Eq. (16) only requires *counting measurements* [18]. Therefore, this shape factor has been widely applied, including various modifications. Modern stereological tools [30] allow determination in a fairly easy way of N_V, but the approach is based on the production of two parallel sections on close distance. This can be realized by scanning tunneling microscope, or is readily realized in translucent materials. In concrete technology this would require significant extra labor of high quality. Of course, when particle size is already known, N_V can easily be estimated by means of Eq. (8).

5. Illustrative application to different types of aggregates

Two types of aggregate, fluvial gravel and crushed rock, respectively, were investigated for illustration purposes in this study. Since examples of image analysis approaches to *sections* are most common in the international literature, we have selected the projection image approach for this illustrative example. For each type of aggregate, 18 particles were selected and subjected to conventional image analysis, and to stereological estimations in this paper. The selected particles are within a narrow size range around 18 mm (see Fig. 6) so as to eliminate the effect of size variations. The measurement results are averaged over the 18 particles for each aggregate group. The *projection profiles* are measured by automatic image analysis and the shape parameters listed in Section 4.2 are calculated (Table 1).

The circularity is 1 for a circle in a plane (2D), and higher (>1) for irregular shapes. The circularity of the particle projection profiles for the fluvial gravel (1.257) is lower than that of the crushed rock (1.359), indicating that the boundary of the fluvial gravel particles is more conforming to ellipse type. The sphericity ratio is 1 for a sphere in space (3D), and lower (<1) for irregular shape. The sphericity ratio for the fluvial gravel is slightly higher than that of the crushed rock, confirming that the latter aggregate type is more angular than the other. The quasi-3D shape parameters at the bottom of Table 1 (in particular, flakiness ratio and shape factor) reveal relatively high sensitivity, since differences in outcomes between the two aggregate types are of the order of 20%.

Table 1
Shape parameters obtained by quantitative analysis of projection image

Aggregate type	Fluvial gravel	Crushed rock
Area (cm^2)	2.427	2.823
Perimeter (cm)	6.120	6.914
Max axis length (cm)	2.067	2.293
Breadth (cm)	1.563	1.812
Arithmetic mean of elongation ratio (LENGTH/BReadth)	1.330	1.281
Weighted mean of elongation ratio	1.315	1.276
Aspect ratio (F_{max}/F_{min})	1.367	1.355
Circularity [$Perimeter^2/(4\pi \times Area)$]	1.257	1.359
Rectangularity (area/area of bounding rectangle)	0.730	0.682
Fullness [$area/(F_{min} \times F_{max})$]	0.733	0.712
Flakiness ratio λ (thickness/breadth)	0.393	0.325
Sphericity ratio	0.607	0.591
Shape factor	0.342	0.290

The stereological methods described in Section 4.3 were also applied to the particles. In fact, the average tangent height $\overline{H_2}$ equals the Feret diameter averaged over all orientations. To simplify the procedures, $\overline{H_3}$ is averaged over thickness, length and breadth. Since size distribution of aggregate particles is not taken into consideration in this paper, only near mono-sized particles are analysed. This means that moments of the particle size distribution defined in Eq. (15) are simplified to

$$M_3(d) = (\overline{H}_3)^3, \quad M_2(d) = (\overline{H}_3)^2, \quad M_1(d) = \overline{H}_3 \tag{17}$$

This allows easy calculation of the shape indices s_1^*, s_2 and s_3 (Table 2). However, it should be noted that the stereological descriptors introduced in Section 4.3 are *readily applicable to more complicated cases of multi-size particle samples* (e.g., coarse aggregate conforming to Fuller-type size distribution, or cement particles conforming to Rosin–Rammler size distribution).

The investigated two groups of aggregate particles are in the same size range, so the size parameters, such as the average tangent heights in 3D $\overline{H}_3$, and the specific surface area, are expected to be similar (see Table 2). The shape factors s_3 and s_2 are 0.524 and 3.14, respectively for spheres. The closer the measurement to these values, the more the investigated particles approximate spheres. Table 2 reveals that the fluvial gravel comes closer to the spherical shape. This confirms that the coarse aggregates of fluvial origin can be reasonably replaced by spherical particles in computer simulation of particle packing in concrete [31,32]; however, a simulation based on ellipsoids will surely provide

Fig. 6. Representative particles from fluvial gravel (left) and from crushed rock (right); the particles are numbered as indicated in the table.

Table 2
Shape parameters obtained by stereological methods

Aggregate type	Fluvial gravel	Crushed rock
Mean volume per particle $\overline{V}$ (cm^3)	1.590	1.673
Area of projection profile $\overline{A}$ (cm^2)	2.427	2.823
Perimeter of projection profile $\overline{L}_P$ (cm)	6.120	6.914
Specific surface area $\overline{S}/\overline{V}$ (cm^{-1})	3.211	3.118
Mean surface per particle $\overline{S}$ (cm^2)	5.105	5.216
$\overline{L}_3 = 4\overline{V}/\overline{S}$ (cm)	1.246	1.283
$\overline{H}_3$ (cm)	1.411	1.571
$\overline{H}_2$ (cm)	1.814	2.039
Surface curvature $\overline{\kappa}_S$ (cm^{-1})	0.866	0.770
s_3	0.566	0.431
s_2	2.564	2.113
s_1^*	0.883	0.816

better results. The ratio between the crushed rock and the fluvial gravel for s_1^*, s_2 and s_3 is 0.92 (=0.816/0.883), 0.82 (=2.113/2.564) and 0.76 (=0.431/0.566), respectively. The difference between the two aggregate types is increasing with the involved dimensions. This implies that a higher order shape parameter (in this case s_3) is more suitable for the purpose of distinguishing aggregate types in terms of shape, since it contains more shape information (in three dimensions) of the investigated particles. The Underwood shape parameter in Eq. (16) only distinguished the aggregates by values about 4% different.

Note that a second publication will complete the presented methodology by discussing more pragmatic methods used for shape assessment. Further, it will introduce innovative and efficient but less intuitive methods for shape assessment based on Fourier transformation. The illustrative example dealing with shape assessment of two different types of non–embedded aggregate particles presented herein will be extended to such approaches. This will allow making more general comparative statements as to reliability, sensitivity and efficiency of shape assessment approaches.

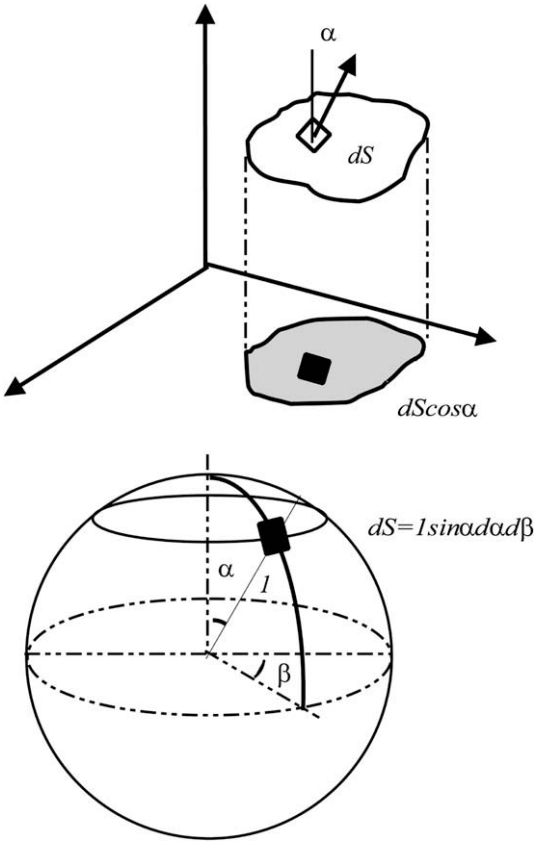

Fig. 7. Principles of geometric global averaging applied to surface area in 3D space, requiring randomization of angle β and of $\sin\alpha$.

6. Conclusions

The traditional quantitative image analysis approach to shape assessment is 2D, and can handle non–embedded particles, or particles embedded in a cementitious matrix. The illustrative example reveals systematic differences between the two aggregate types. The quasi-3D shape parameters at the bottom of Table 1 (in particular, flakiness ratio and shape factor) reveal relatively high sensitivity, since differences in outcomes between the two aggregate types are of the order of 20%.

Stereology offers powerful relationships based on geometrical probability theory that offer possibilities for estimating in an efficient and sensitive way 3D shape of particles. Of course, the researcher should strive for the assessment of 3D shape parameters because of their more realistic nature. The methods are versatile; the solution strategy can be attuned to the application. Ref. [33], for example, presents an interesting application of stereological estimation based on quantitative image analysis in concrete technology.

To efficiently provide unbiased representative information on 3D particle shape, the sampling strategy should be carefully designed. In the given example, the ratio between the outcomes for crushed rock and for the fluvial gravel for the shape indices s_1^*, s_2 and s_3 is 0.92, 0.82 and 0.76, respectively. Hence, the difference between the two aggregate types is increasing with the involved dimensions. This implies that a higher order shape parameter (in this case s_3) is more sensitive in distinguishing aggregate types in terms of shape, since it contains more shape information (in three dimensions) of the investigated particles. This single parameter is also superior to the Underwood shape parameter given by Eq. (16).

Appendix A. Global averaging of geometric features

Since the probability of intersection of a grid line and an infinitesimal small trace element in a plane (2D approach), or an infinitely small surface element (3D approach) is proportional to their extensions perpendicular to the grid line (Fig. 7), we have

$$\bar{P}_L = L_A \frac{\int_0^{\pi/2} \cos\alpha \mathrm{d}\alpha}{\int_0^{\pi/2} \mathrm{d}\alpha} = \frac{2}{\pi} L_A \quad \text{and}$$

$$\bar{P}_L = S_V \frac{\int_0^{\pi/2}\int_0^{\pi/2} \cos\alpha \sin\alpha \mathrm{d}\alpha\mathrm{d}\beta}{\int_0^{\pi/2}\int_0^{\pi/2} \sin\alpha \mathrm{d}\alpha\mathrm{d}\beta} = \frac{1}{2} S_V$$

These are the constants in Eqs. (2) and (3), respectively.

Appendix B. Additional 3D shape indices

$$\frac{s_{-1}s_2^2}{s_3} = \frac{4\pi N_A P_L}{N_V P_P} \frac{M_3(d)}{M_2^2(d) M_{-1}(d)}$$

$$\frac{s_1^2}{s_2} = \frac{N_A^2}{2 P_L N_V} \frac{M_2(d)}{M_1^2(d)}$$

$$\frac{s_2^2 s_1}{s_3} = \frac{4 N_A P_L^2}{N_V^2 P_P} \frac{M_3(d)}{M_2^2(d) M_1}$$

$$\frac{s_2^3}{s_3^2} = \frac{S_V^3}{V_V^2 N_V} \frac{M_3^2(d)}{M_2^3(d)} = \frac{8 P_L^3}{P_P^2 N_V} \frac{M_3^2(d)}{M_2^3(d)}$$

$$s_1^* s_{-1} = \frac{8\pi V_V N_A}{S_V^2} \frac{M_{-1}^{-1}(d)}{M_1(d)} = \frac{2\pi P_P N_A}{P_L^2} \frac{M_{-1}^{-1}(d)}{M_1(d)}$$

These indices contain the stereological parameter N_V that is difficult (though not impossible) to determine for aggregate embedded in a cementitious matrix, so could only suitably be used for loose particles.

References

[1] Goldman A, Bentur A. The influence of micro-fillers on enhancement of concrete strength. Cement Concrete Comp 1993;23:962–72.
[2] Detwiler RJ, Mehta PK. Chemical and physical effects of silica fume on the mechanical behavior of concrete. ACI Mater J 1989;86(6):609–14.
[3] Bui DD, Hu J, Stroeven P. Particle size effect on the strength of rice husk ash blended gap-graded Portland cement concrete. Cement Concrete Comp 2005;27(3):357–66.
[4] Orange G, Dugat J, Acker P. DUCTAL: new high performance concretes. Damage resistance and micromechanical analysis. In: Rossi P, Chanvillard G, editors. Fibre reinforced concretes BEFIB'2000. Cachan: RILEM Publ; 2000. p. 781–90.
[5] Mora CF, Kwan AKH, Chan HC. Particle size distribution analysis of coarse aggregate using digital image processing. Cement Concrete Res 1989;28(6):921–32.
[6] Jamkar SS, Rao CBK. Index of aggregate particle shape and texture of coarse aggregate as a parameter for concrete mix proportioning. Cement Concrete Res 2004;34:2021–7.
[7] Basheer PAM, Long AE, Basheer L. Establishing the interactive effects of aggregate size, shape and type on properties of concrete. <http://www.qub.ac.uk/civeng/research/Intro/research_areas/durability/mixeffects1.html>.
[8] Underwood EE. Quantitative stereology. Addison-Wesley; 1970.
[9] Stroeven P. A stereological approach to roughness of fracture surfaces and tortuosity of transport paths in concrete. Cement Concrete Comp 2000;22:331–41.
[10] Coster M, Chermant J-L. Recent developments in quantitative fractography. Int Met Rev 1983;28:228–50.
[11] Gokhale AM, Underwood EE. A general method for estimation of fracture surface roughness: Part 1. Theoretical analysis. Metall Trans A 1990;21A:1193–9.
[12] Kendall DG, Baeden D, Carne TK, Le H. Shape and shape theory. New York: Wiley & Sons; 1999.
[13] Hu J, Stroeven P. Shape characterization of concrete aggregate. Im Anal Stereol 2006;25:43–53.
[14] Stroeven P. Stereological estimates for roughness and tortuosity in cementitious composites. Im Anal Stereol 2000;19:67–70.
[15] Hu J, Stroeven P. Local porosity analysis of pore structure in cement paste. Cement Concrete Res 2005;35(2):233–42.
[16] Nemati KM, Stroeven P. Stereological analysis of micromechanical behavior of concrete. Mater Struct 2000;34:486–94.
[17] Stroeven P. Design of experiments in concrete technology: influx of materials science and stereology. In: Chraponski J, Cwajna J, Wojnar L, editors. Proceedings 9th European Congress on Stereology and Image Analysis (Poland). Krakow: Polish Society for Stereology; 2005. p. 44–54.
[18] Stroeven P, Hu J. Stereology: historical perspective and applicability to concrete technology. Mater Struct 2006;39:127–35.
[19] Steinhaus H. Akademie der Wissenschaften Leipzig, Berlin 1930;82:120–30.
[20] Kendall MG, Moran PAP. Geometric probability. London: Butler & Tanner Ltd; 1963.
[21] Stroeven P. Some aspects of the micromechanics of concrete. PhD thesis, Delft: Delft University Press; 1973.
[22] DeHoff RT. Stereological information contained in the integral mean curvature. J Microsc (Wien) 1980;37(Suppl.):32–6.
[23] Stroeven P. Automatic quantification of microcracks network by stereological method of total projections in mortars and concretes by Ringot E. Discussion. Cement Concrete Res 1988;18:657–9.
[24] Saltikov SA. Stereometric metallography. 2nd ed. Moscow: Metallurgizdat; 1945.
[25] ASTM D 3398-97. Standard Test for Index of Aggregate Particle Shape and Texture. West Conshohocken: USA; 1997.
[26] Yamamoto H, Matsuyama T, Wada M. Shape distinction of particulate materials by laser diffraction pattern analysis. Powder Technol 2002;122:205–11.
[27] Kwan AKH, Mora CF, Chan HC. Particle shape analysis of coarse aggregate using digital image processing. Cement Concrete Res 1999;29:1403–10.
[28] Stroeven P. Analytical and computer-simulation approaches to the extent of the interfacial transition zone in concrete. In: Brandt AM, Li VC, Marshall IH, editors. Proceedings brittle matrix composites 6. Cambridge: Woodhead Publishing; 2000. p. 465–84.
[29] Underwood EE. Three-dimensional shape parameters from planar sections, NBS Spec Publ 431, Fourth int congress for stereology. Washington: US Printing Off; 1976. p. 91–2.
[30] Gundersen HJG et al. Some new, simple and efficient stereological methods and their use in pathological research and diagnosis. Acta Pathol Mic Sci 1988;96:379–94.
[31] Stroeven P, Stroeven M. SPACE approach to concrete's space structure and its mechanical properties. Heron 2001;46(4):265–89.
[32] Stroeven M. Discrete numerical modelling of composite materials – application to cementitious materials. PhD thesis, Delft: Delft University; 1999.
[33] Stroeven P, Hu J. Gradient structures in cementitious materials. Cement Concrete Comp 2007;29(4):313–23.